



13th World Conference on Earthquake Engineering
Vancouver, B.C., Canada
August 1-6, 2004
Paper No. 1707

EXPERIMENTAL OBSERVATION OF AXIAL LOAD EFFECTS IN ISOLATION BEARINGS

Keri L. RYAN¹, James M. KELLY² and Anil K. CHOPRA³

SUMMARY

In previous studies, the response characteristics of rubber bearings were observed to be influenced by the weight or axial load they carried. Such influence is important since axial loads vary in an earthquake due to overturning. However, the particular effects of axial load on the bearing response are not well understood, and we can benefit from additional data. In this paper, response data from characteristic tests on three different types of bearings – two high-damping rubber and one lead-rubber bearing – is presented. This data demonstrates that the bearing lateral stiffness decreases with increasing axial load, while its vertical stiffness decreases with increasing lateral deformation. Stiffness values derived from linear stability theory are shown to correlate to the observed stiffnesses. In addition, the yield strength of lead-rubber bearings is observed to degrade significantly as the bearing unloads axially. An empirical model has been devised to represent this strength degradation. The data presented here, as supported by theory, forms the basis for development of a dynamic bearing model that includes the axial load effects.

INTRODUCTION

Varying axial loads have been observed to affect the response characteristics of rubber bearings; this effect is not usually accounted for in dynamic analysis. First, in several types of rubber bearings, the lateral stiffness has been observed to decrease with increasing axial load (Griffith [1], Kelly [2], Aiken [3]). Rubber bearings have also been shown to soften in the vertical direction at large lateral deformations; in recent projects, bearings under large lateral deformation were “jacked up” with no evidence of the cavitation damage that results in pure tension (Clark [4], Kelly [5]). Although less documented, the yield strength of a lead-rubber bearing, or strength of the lead core, has been observed to vary with axial load, such that a lightly loaded bearing may not achieve its theoretical strength (Tyler [6], Hwang [7]).

In conjunction with research supported by the Earthquake Engineering Research Center (EERC) and Shimuzu Corporation, isolation bearings were designed for earthquake simulator tests of a reinforced-concrete model of a three-story building in Sendai, Japan. Prototype high-damping rubber (HDR) bearings (from Bridgestone Corporation and Malaysian Rubber Products Research Association or MRPRA)

¹Grad. Stud., Dept. of Civ. and Envir. Engrg., Univ. of California, Berkeley, Berkeley, CA 94720.

²Prof. Emeritus, Dept. of Civ. and Envir. Engrg., Univ. of California, Berkeley, Berkeley, CA 94720.

³Johnson Prof., Dept. of Civ. and Envir. Engrg., Univ. of California, Berkeley, Berkeley, CA 94720.

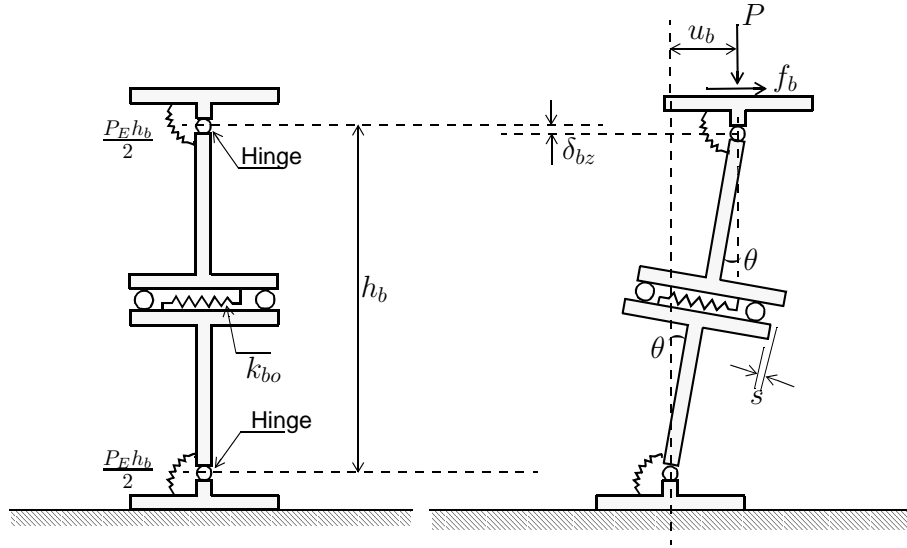


Figure 1: Two-spring model of an isolation bearing in the undeformed and deformed configuration.

and lead-rubber (LRB) bearings (from Oiles Industry Co.) were tested to determine their mechanical characteristics. Details of the experimental test program – which was performed over 10 years ago – and some results were published (Clark [4], Aiken [8]); but much of the test data, especially for MRPRA and Oiles bearings, was never reported.

Our objective is to use this untapped resource to confirm and better understand the interaction of lateral and vertical force-deformation in rubber and lead-rubber bearings. The effects of this interaction, which include variation of lateral stiffness and yield strength with axial load, and variation of vertical stiffness with lateral deformation, are hereafter referred to as “axial load effects”. The observed lateral and vertical stiffness variation is compared to theoretical stiffness equations determined from linear stability analysis, and an empirical equation is suggested to represent the strength variation in lead-rubber bearings. The data provides a basis for future development of a dynamic model of isolation bearings that includes axial-load effects.

THEORETICAL BEARING FORCE-DEFORMATION RELATION

The axial load effects described above can be theoretically explained by stability analysis of a multi-layer bearing, or alternatively, by a simplified two-spring model of the bearing (Kelly [9]) that results in explicit force-deformation relations. The two-spring model (Fig. 1) is a composition of rigid tees connected by a rotational spring, subdivided at top and bottom, and a shear spring with frictionless rollers at midheight. The bottom plate is fixed and the top plate is constrained against rotation. Axial flexibility of the bearing is included by an additional vertical spring in series (not shown in Fig. 1).

Analysis of the linear two-spring model, originally presented in Kelly [9], leads to the following principle results:

1. The critical buckling load of the bearing is

$$P_{cr} \approx \pm \sqrt{P_S P_E} \quad (1)$$

where $P_S = GA_s$ and $P_E = (\pi^2/h_b^2)EI_s$ is the conventional Euler buckling load of a column, incorporating the bearing properties: shear modulus G , cross-sectional area A_s (modified to account for the undeforming steel layers), height h_b , and bending stiffness EI_s . Equation 1 approximates the buckling load determined from stability analysis of a multi-layer bearing (Kelly [9, Eq. 8.12]), with a reasonable assumption that $P_E \gg P_S$.

2. The lateral force f_b as a function of the deformation u_b is given as (Kelly [9, Eq. 8.33])

$$f_b = k_b u_b \quad k_b = k_{bo} \left[1 - \left(\frac{P}{P_{cr}} \right)^2 \right] \quad (2)$$

where $k_{bo} = P_S/h_b$ is the nominal shear stiffness and P is the current axial force on the bearing. The lateral stiffness k_b in Eq. 2 for the two-spring model is a good approximation to the stiffness derived from stability analysis of a multi-layer bearing (Kelly [9, Fig. 8-4]). Physically, Eq. 2 represents a reduction in the lateral stiffness as the axial force P approaches the critical load P_{cr} , which holds for both compressive and tensile loads P (Kelly [5]).

3. The axial or vertical force P as a function of the vertical deformation u_{bz} is approximated as

$$P = k_{bz} \left(u_{bz} - \frac{P_S}{P_E} \frac{u_b^2}{h_b} \right) \quad (3)$$

with incremental, or tangent vertical stiffness k_{bz} given by Kelly [9, Eq. 8.35]:

$$k_{bz} = k_{bzo} \left(1 + \frac{3u_b^2}{\pi^2 r_b^2} \right)^{-1} \quad (4)$$

reduced to this form by substituting P_E in terms of h_b and EI_s , where k_{bzo} is the nominal vertical or axial stiffness and r_b is the bending radius of gyration (bending inertia $I_s = A_s r_b^2$). Equation 4 implies a vertical softening of the bearing relative to its nominal vertical stiffness, which occurs due to tilting of the bearing reinforcing layers under shear deformation, meaning the axial loads are resisted in part by shear.

AXIAL-LOAD VARIED TESTS

Interpretation of Experimental Data

The axial-load varied tests allows observation of how the stiffness and strength of the bearings vary with axial load. In these tests, two bearings from each manufacturer were subjected to the prescribed lateral deformation, five cycles each at shear strains (lateral deformation relative to height) of 5, 25, 50, 75 and 100%. The tests were repeated at axial loads of 0, $P_{st}/2$, P_{st} , $2P_{st}$, $3P_{st}$ and $-P_{st}/10$, one bearing each for design loads P_{st} of 78 kN (interior bearing) and 49 kN (exterior bearing). The tensile tests were omitted for the Oiles LRB bearing, attached by a doweled rather than a bolted connection. For reference, the dimensions of the three prototype bearings are listed in Table 1.

The data was analyzed as follows: the lateral force in the bearing in response to the applied deformation was recorded; this force signal was smoothed using a Gaussian kernel with full width at half maximum (FWHM) equal to $4*\delta t$. From the deformation and force signals, the force-deformation relation (bearing hysteresis) for each test was plotted at the various strain levels. As an example, force-deformation for the Bridgestone bearing at the axial load $P = P_{st}$ is shown in Fig. 2.

Table 1: Dimensions of Prototype Bearings

Property	Bridgestone	MRPRA	Oiles
Bonded diameter D (mm)	176	140	180
Lead core diameter D_l (mm)	-	-	25
Rubber thickness per layer t (mm)	2.2	4.0	3.0
Number of rubber layers n_r	20	12	21
Total rubber thickness t_r (mm)	44	48	63
Thickness per steel shim t_s (mm)	1.0	1.6	1.0
Number of steel shims n_s	19	11	20
Total bearing height h_b (mm)	63	65.6	83
Cross-section area A (mm ²)	24,388	15,394	25,447
Shape factor S	20	8.75	15

In reality, the bearing properties vary with shear strain; thus, from the bearing force-deformation, the lateral strength and stiffness at each strain level were determined independently. The proposed equation for stiffness k_b (Eq. 2) ignores strain dependence, but so do typical models for LRB bearings because the strain dependence is minor and properties at large strains control the peak response of the system. Locating the positive and negative y -axis force intercepts in each cycle and averaging over the cycles, the strength Q was interpreted as half the distance between the averaged intercepts, which are indicated by dots in Fig. 2. Computed from data points adjacent to these force intercepts, the post-yield stiffness k_y was interpreted as the slope at the force intercepts, averaged over the cycles. Although the theoretical variation of k_y (Eq. 2) is based on linear analysis, the post-yield stiffness is used instead because the bearing behavior is observed to be nonlinear. For the Bridgestone example, the resultant stiffnesses are the slopes of the dashed lines drawn through the force intercepts (Fig. 2). Also computed at each strain level, the nominal stiffness k_{bo} was interpreted as the observed stiffness at zero axial load (not shown here), and the critical load P_{cr} (Eq. 1) was computed from the observed nominal shear modulus G_o .

While this procedure worked well for the Bridgestone and MRPRA bearings, some adjustments were necessary for the Oiles bearings. A sample force-deformation for Oiles Bearing 1 at $P = P_{st}$ (Fig. 3) shows a slight pinching of the hysteresis near the origin, i.e., zero shear strain. In this case, the stiffness was interpreted as the average secant stiffness over a larger range, from about -63 to +63% of the maximum local strain. Again, the resulting stiffness is shown as the slope of the dashed lines in Fig. 3.

The Oiles data at zero axial load ($P = 0$) presented another challenge, as the post-yield stiffness is influenced by the near complete loss of strength (Fig. 4). Although not theoretically predicted, the interaction between rubber and lead appears to cause the tangent stiffness to decrease at the origin compared to large shear strains. Thus, how should the stiffness, representative of the nominal stiffness, be interpreted to give values consistent with those for nonzero axial loads? Believing the low stiffness near the origin to be an anomaly, we took the stiffness as the average tangent at about 63% of the maximum local strain, determined from adjacent data points at that strain. This stiffness, shown drawn through the points about which it was estimated (Fig. 4), appears to be indicative of the tangent stiffness away from the origin.

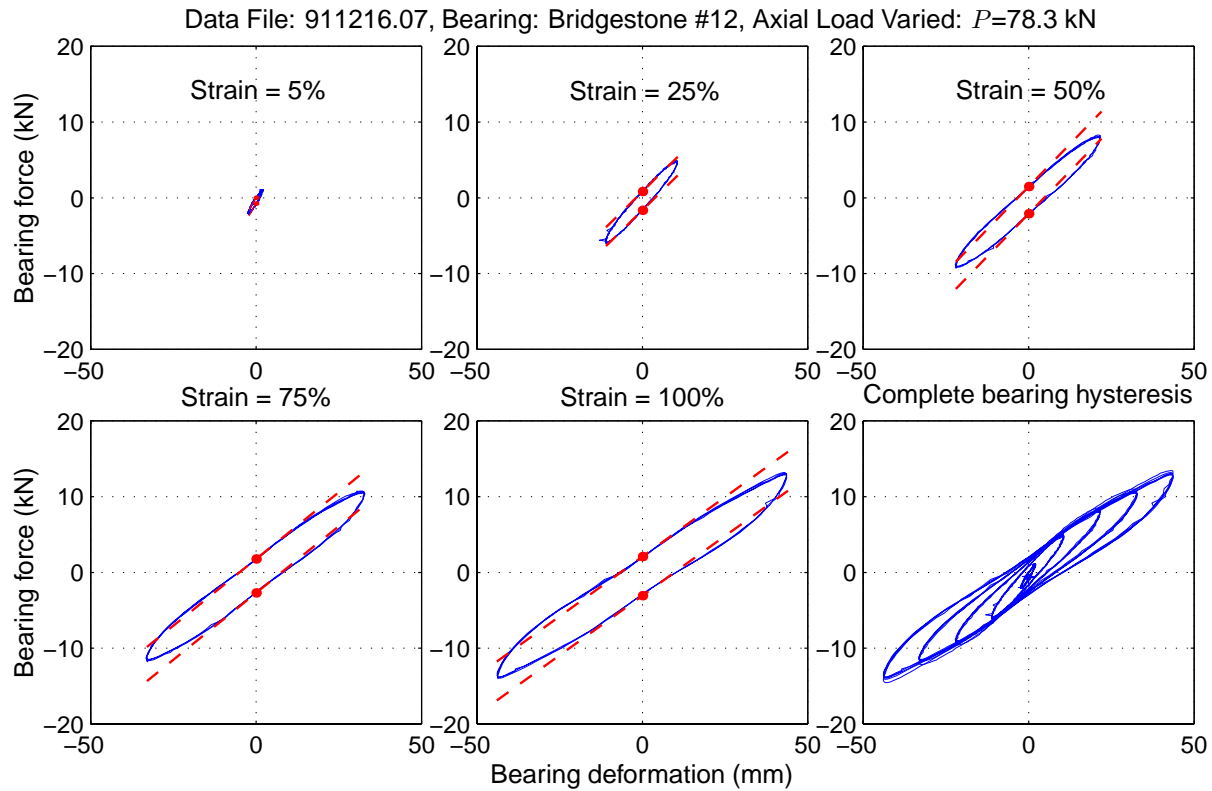


Figure 2: Lateral force-deformation at different strain levels and complete bearing hysteresis for Bridgestone #12 with applied axial load $P = 78$ kN. Interpretation of Q and k_b given by dots at the y -intercept and dashed lines.

Lateral Stiffness

Compiling the test data as described in the previous section, Fig. 5 compares the normalized post-yield stiffness k_b/k_{b0} at different shear strains versus P/P_{cr} for the three different bearings with Eq. 2. For both the Bridgestone (Fig. 5a) and MRPRA bearings (Fig. 5b), the theoretical stiffness (Eq. 2) agrees well with the experimental data, matching best at larger strains where the data is considered to be most reliable. Data for the Oiles bearings (Fig. 5c) agrees less with Eq. 2, partly due to the difficulty of obtaining a reliable estimate of the nominal stiffness k_{b0} from the test data. (Recall that a different method was used to determine the nominal stiffness than the stiffness at nonzero axial loads). However, the slope of the experimental curves appear to match Eq. 2. Considering the many possibilities for experimental error, the theoretical model and experimental results seem to be in satisfactory agreement.

On a side note, observe that the range of P/P_{cr} is different for each bearing, though they are tested under identical axial loads P . The critical load P_{cr} can be shown to be a linear function of the bearing shape factor S , equal to $D/4t$ for a circular bearing with diameter D and thickness t of individual rubber layers (Kelly [9]). Thus, the wide range of shape factors for the bearings (S between 8.75 and 20, listed in Table 1), led to significant variations in the critical load P_{cr} (Eq. 1). Figure 5 shows that the stiffness variation due to axial loads is greater in bearings with low shape factors, or thick rubber layers relative to their size, like MRPRA, than in bearings with high shape factors, like Bridgestone.

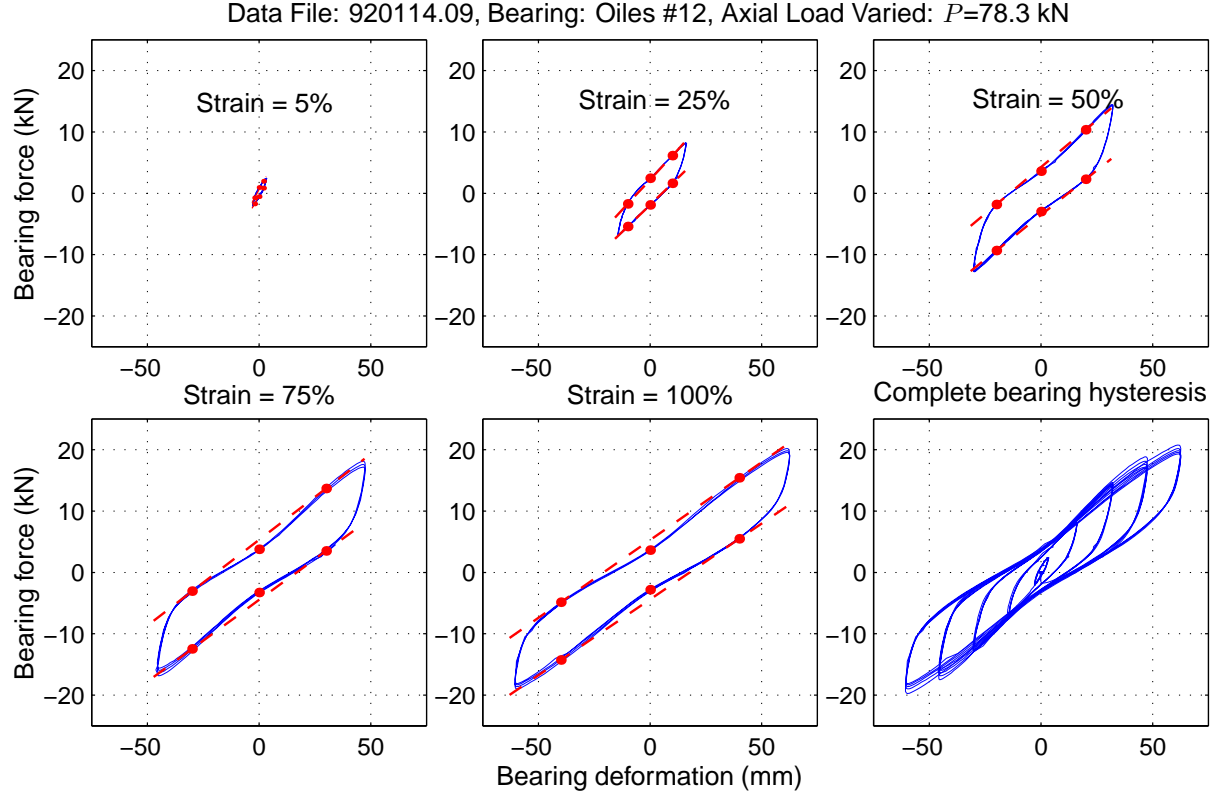


Figure 3: Lateral force-deformation at different strain levels and complete bearing hysteresis for Oiles #12 with applied axial load $P = 78$ kN. Interpretation of Q and k_b given by dots at the y -intercept and dashed lines.

Lateral Strength

Similar to observations in other research (Tyler [6], Hwang [7]), our data for LRB bearings demonstrated a variation in the yield strength with axial load. From the compiled test data, the observed strength at different shear strains is plotted as a function of the axial load for two different Oiles bearings (Fig. 6). As the axial load P is decreased from its maximum value, the strength Q appears to degrade slowly at first, and then drop suddenly as P approaches zero.

This observation that a LRB bearing fails to achieve its full strength when lightly loaded has not, to our knowledge, been verified by mechanical analysis. However, we have developed an empirical equation for the yield strength as a function of the compressive load P to match the experimental data:

$$Q = Q_o \left(1 - e^{(-P/P_o)} \right) \quad (5)$$

where Q_o is the nominal yield strength of the bearing, achievable with an adequate confining pressure; and P_o is the axial load corresponding to about 63% of nominal strength. When the bearing is in tension ($P < 0$), the effective yield strength is taken to be zero because the lead core tends to rotate instead of shearing.

To apply this model to the data for the Oiles bearing, the nominal strength Q_o at each strain level was taken to be the observed strength of the first bearing at its largest applied load ($3P_{st} = 235$ kN), and the load P_o

Data File: 920114.07, Bearing: Oiles #12, Axial Load Varied: $P=0$ kN

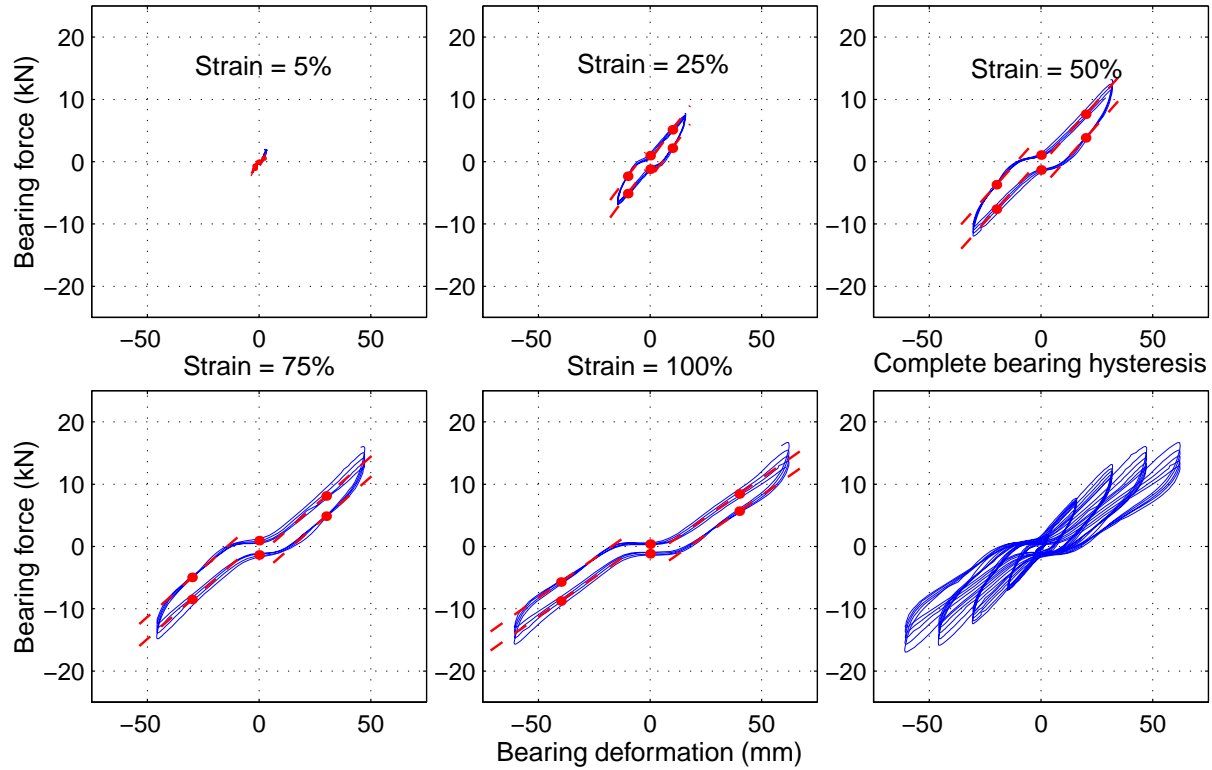


Figure 4: Lateral force-deformation at different strain levels and complete bearing hysteresis for Oiles #12 with applied axial load $P = 0$ kN. Interpretation of Q and k_b given by dots at the y -intercept and dashed lines.

for each bearing was selected visually to best fit the data. (Note that the strength is normalized by Q_0 and the axial load is normalized by P_0 in Fig. 6). P_0 should be the same for both bearings, which are nominally identical; thus a difference in observed values of P_0 (30 kN and 20 kN) may be due to accidental variation and testing under different axial loads ($P_{st} = 78$ kN and 49 kN, for Bearing 1 and Bearing 2, respectively).

The proposed empirical model (Eq. 5) is depicted as a solid line in Fig. 6, and proves to be a reasonable fit to the bearing data, especially at the larger strains where the data is more reliable. While the observed strength does not reduce to zero, it does fall exponentially as axial load is removed. It was documented that at zero axial load the lead core began to extrude out of both ends of the bearing during testing, seeming to support our claim that the lead core is ineffective in tension. However, the Oiles bearings could not be tested in tension because they were attached by doweled connections, which may or may not have contributed to the extrusion of the lead core.

VERTICAL TESTS

Interpretation of Experimental Data

Vertical characteristic tests are considered primarily to understand damping in the vertical direction. In these tests, a cyclic force-controlled loading in the range $P_{st} \pm 0.3P_{st}$ ($P_{st} = 78$ or 49 kN) was applied to each bearing, and its vertical deformation was recorded. This characteristic test was applied to 15 each

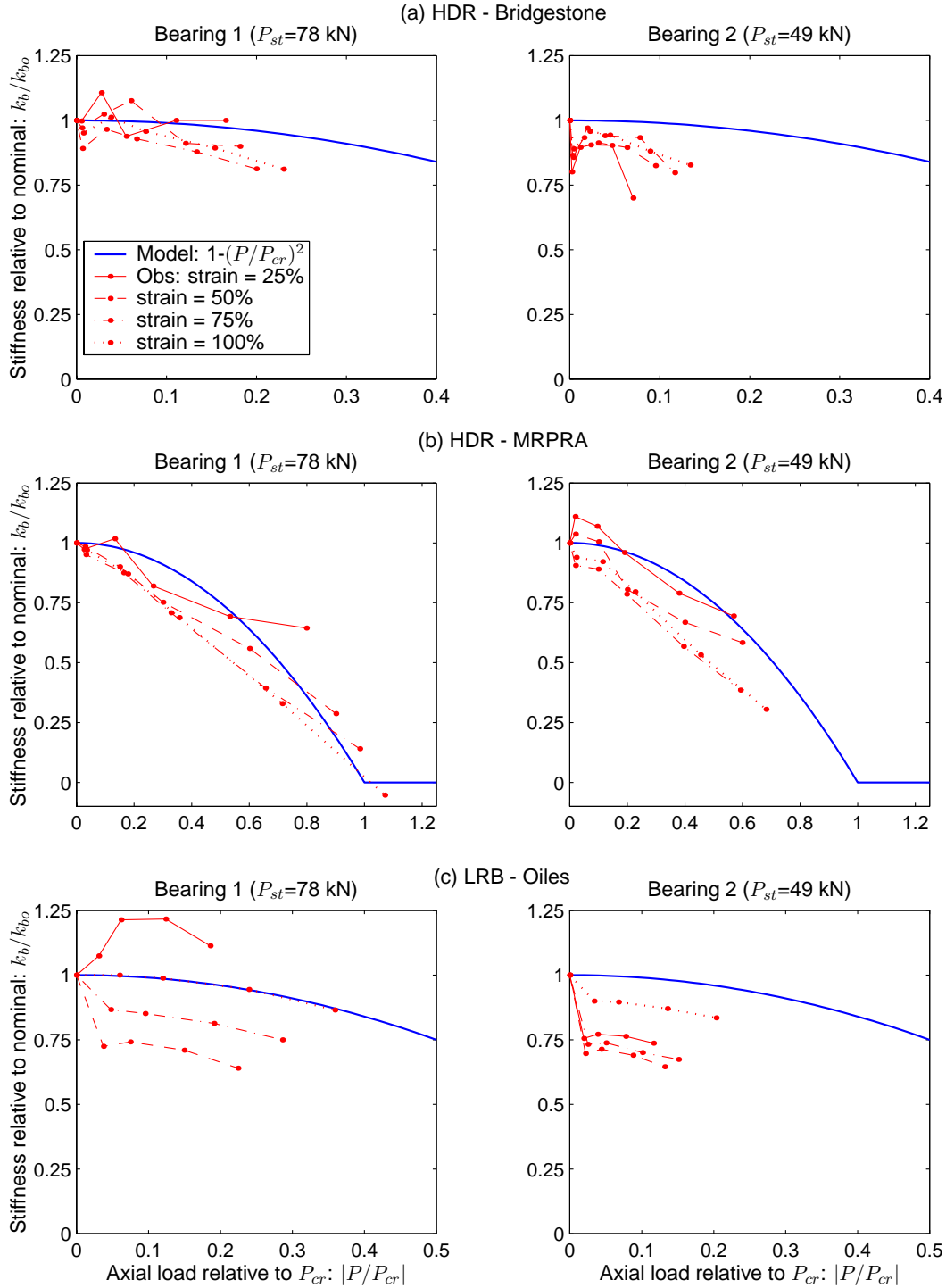


Figure 5: Experimentally observed stiffness ratio k_b/k_{bo} vs P/P_{cr} for (a) Bridgestone HDR, (b) MRPRA HDR, and (c) Oiles LRB, compared with Eq. 2. Data points at $P = 0, P_{st}/2, P_{st}, 2P_{st}, 3P_{st}$, and $-P_{st}/10$, where P_{st} is the design axial load.

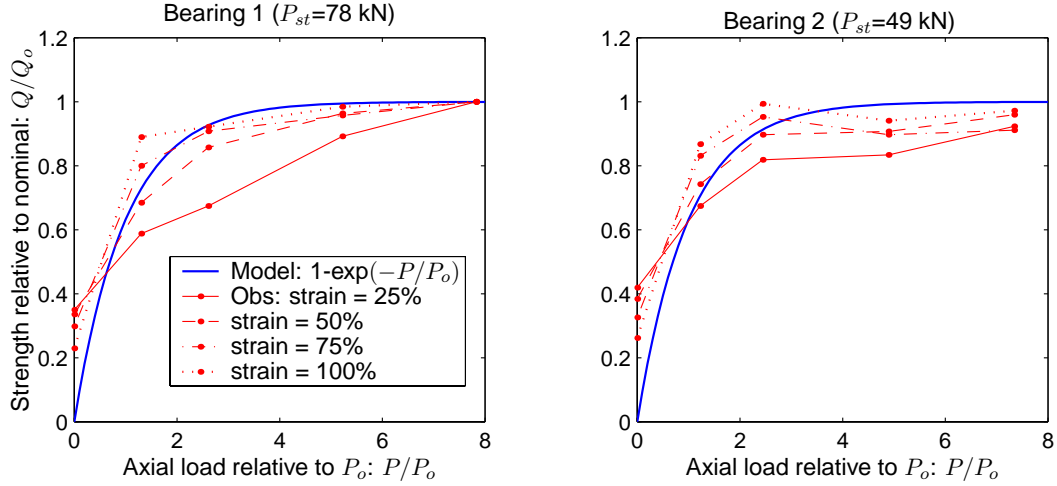


Figure 6: Strength ratio Q/Q_o vs P/P_o for Oiles LRB compared with Eq. 5. Data points at $P = 0$, $P_{st}/2$, P_{st} , $2P_{st}$, and $3P_{st}$, where P_{st} is the design axial load.

of the Bridgestone and Oiles bearings, and 12 MRPRA bearings. Two bearings of each type were also subjected to the offset test, a repeat of the vertical characteristic test at imposed “offset” shear strains of 0, 50, 100, and 150% and over the ranges $P_{st} \pm 0.3P_{st}$ and $P_{st} \pm P_{st}$. The offset tests allowed observation of how the vertical stiffness varies with lateral deformation.

During the vertical characteristic tests and offset tests, the load signal was applied using two vertical actuators. The resulting axial force in the bearing was measured by a single load cell under the bearing, while the vertical deformation was measured by four direct current voltage transducers (DCDTs) attached at the bearing “corners”, and then averaged. The observed deformations were not very accurate for two reasons: first, the transducers measured the relative motion between the top and bottom plates of the test machine, which was influenced by plate bending; second, the vertical bearing deformations were small relative to the resolution of the transducers. This problem was greatest for the Bridgestone bearings, with peak deformations on the order of 0.08 mm (.003 in) and a resolution of only 0.025 mm (.001 in). The obvious effect was incredibly noisy data. A Gaussian kernel was no longer a sufficient filter for smoothing the data, and better results were obtained by applying a low pass filter that eliminated frequencies greater than 1 Hz (the test rate was 0.067 Hz).

Samples of the “smoothed” – though still quite noisy – force-deformation relations from the vertical characteristic tests of Bridgestone bearings are shown in Fig. 7. The vertical deformation at the start of the test, which should have indicated the static deformation, was very inconsistent, and thus the plots were centered at zero deformation. The elliptical appearance of the force-deformation relation (Fig. 7) suggests a viscous energy dissipation associated with vertical motion. Thus, a damping coefficient for vertical motion can be estimated from the dissipated energy E_D , equal to the area of the force-deformation loop:

$$\zeta_{eq} = \frac{1}{4\pi} \frac{E_D}{1/2k_{bz}u_{bz}^2} \quad (6)$$

where k_{bz} is the secant stiffness and u_{bz} is one-half the deformation, which is measured as average peak-to-peak over all cycles.

The viscous damping coefficient was estimated from these characteristic tests by the following steps: (1)

Bridgestone Vertical Characteristic Tests: cycles at $P_{st} \pm 0.3P_{st}$ with $P_{st}=78.3$ kN

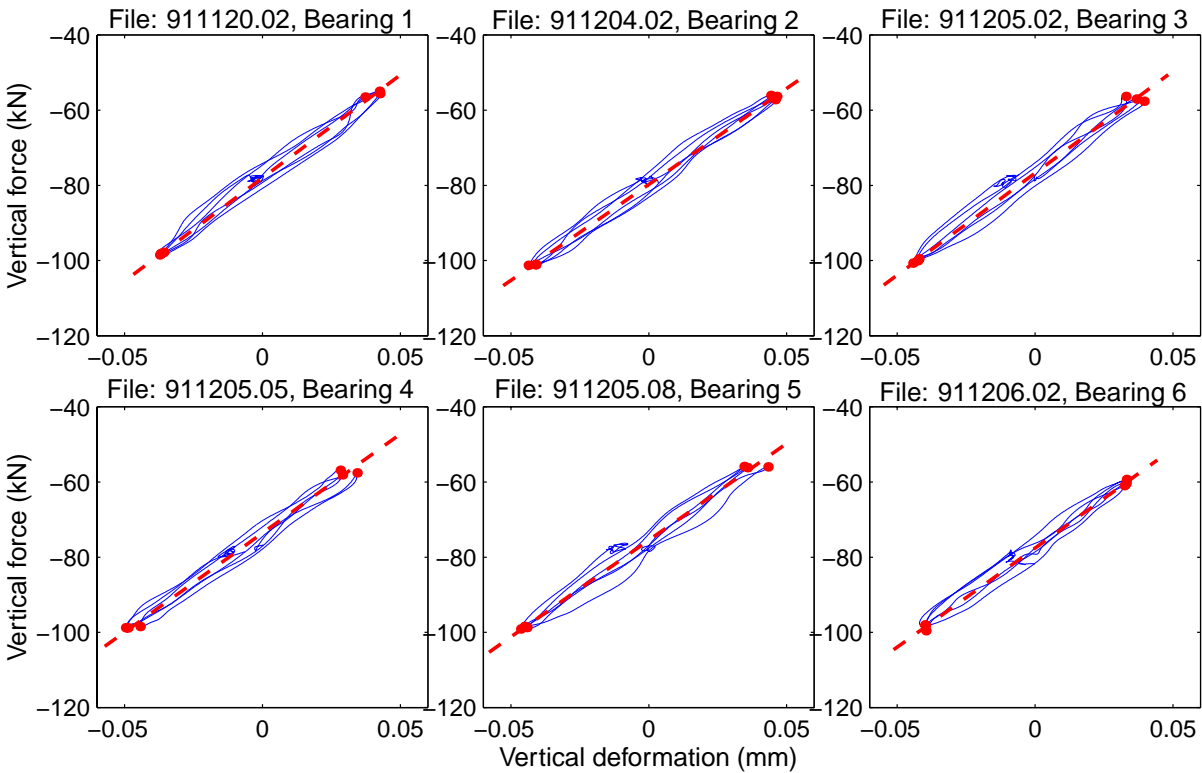


Figure 7: Vertical force-deformation for Bridgestone bearings, as determined from vertical characteristic tests. Interpretation of vertical stiffness k_{bz} given by dashed lines.

locate the local extrema – one at each half-cycle – as the maximum of force*deformation (indicated by dots in Fig. 7), (2) draw a tangent line between each pair of adjacent extreme points, (3) average the slope of this line over all half cycles to get the vertical stiffness (indicated by dashed lines in Fig. 7), (4) estimate the energy dissipated in each half cycle by numerically integrating the area between the tangent line and the actual data, (5) average the energy dissipated over all half cycles and multiply by 2 for energy dissipated per cycle, (6) compute the damping coefficient (Eq. 6) based on the estimates of vertical stiffness, half peak-to-peak deformation, and energy dissipated.

Representative of the offset tests, resulting vertical force-deformation for a Bridgestone bearing is shown for shear strains of 50, 100 and 150% (Fig. 8). Also shown are the dashed lines whose slopes represent the vertical stiffness, determined in the same way as for the vertical characteristic tests. For each load cycle ($P_{st} \pm 0.3P_{st}$, $P_{st} \pm P_{st}$), a slight decrease in stiffness with increasing shear strain is observed.

A peculiar effect was observed in the offset tests for the Oiles LRB bearing (Fig. 9). The response looks normal for load cycles in the range of $P_{st} \pm 0.3P_{st}$, but in the larger range of $P_{st} \pm P_{st}$, the bearing softens rapidly as the axial load approaches zero. The effect is magnified with increase in shear strain. Because the Oiles bearings have dowelled connections, they have a tendency to rollout at the large shear strains. The axial force couple provides a restoring moment to resist rollout. Thus, when the axial force is removed, as in these large range offset tests, significant rollout occurs, and the vertical deformation measurements are affected in unforeseen ways. The proposed model for the LRB bearing does not really address this

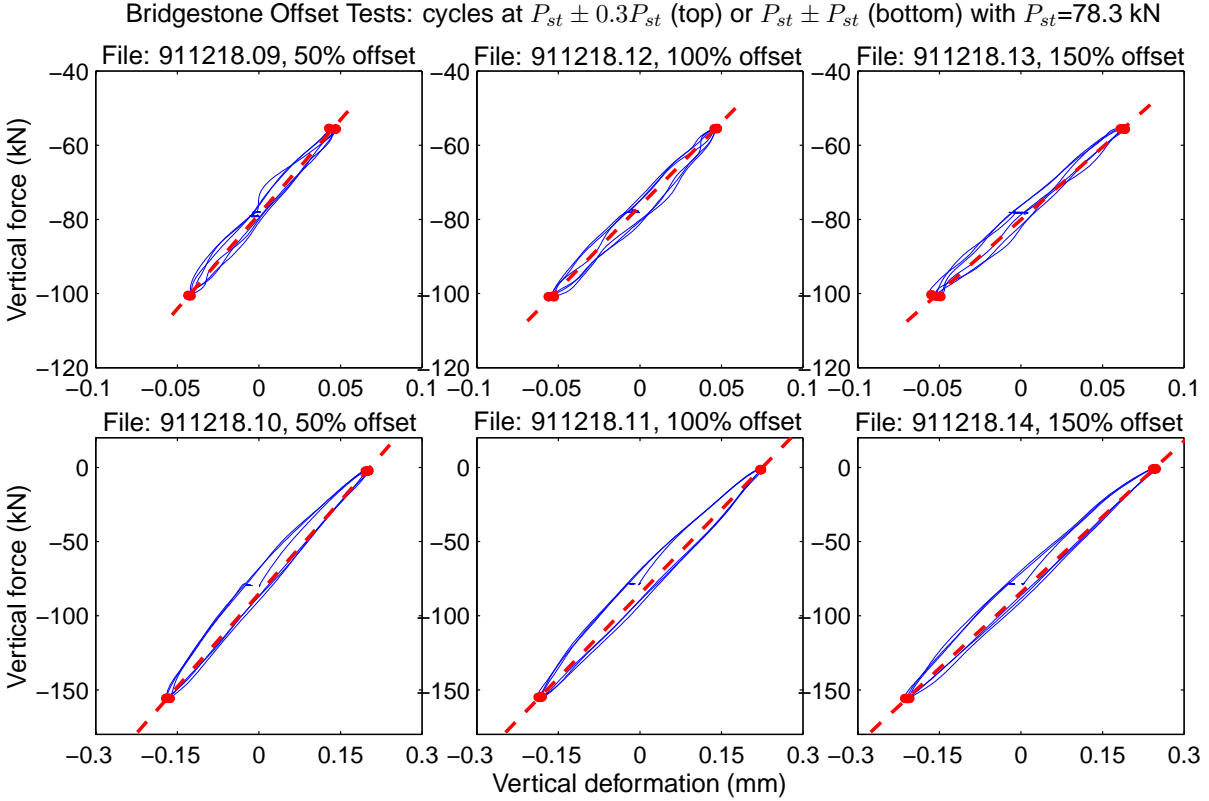


Figure 8: Vertical force-deformation for a single Bridgestone bearing at offset shear strains of 50, 100, 150% and load cycles of $P \pm 0.3P$ or $P \pm P$. Interpretation of vertical stiffness k_{bz} given by dashed lines.

behavior, which is hopefully limited to the increasingly uncommon dowelled connection. We dealt with this by sampling the tangent vertical stiffness at cycles $P_{st} \pm P_{st}$ separately above and below P_{st} (Fig. 9), and using the stiffness at $P > P_{st}$ for comparison with the theoretical stiffness (Fig. 10).

Viscous Damping Coefficient for Vertical Motion

This damping coefficient, determined as described above, was averaged over all characteristic tests for a particular bearing (Bridgestone, Oiles, MRPRA). This resulted in average damping coefficients of $\zeta_{eq} = 0.064, 0.093$ and 0.079 for the Bridgestone, MRPRA, and Oiles bearings, respectively. Damping is observed to increase as the bearing shape factor (Table 1) decreases.

These estimated damping coefficients are not expected to be highly accurate. The energy dissipation, in particular, is likely to be influenced by the noisy data. The numerical integration technique may overestimate the energy dissipation by picking up noise and/or adding area on both sides of the tangent line as positive energy. Furthermore, although interpreted as exactly in-phase, the axial forces and vertical deformations may have been slightly out-of-sync, introducing a phase lag that falsely increases damping. For these reasons, the damping coefficients estimated by this technique may be slightly high, but are believed to give a reasonable impression of vertical damping.

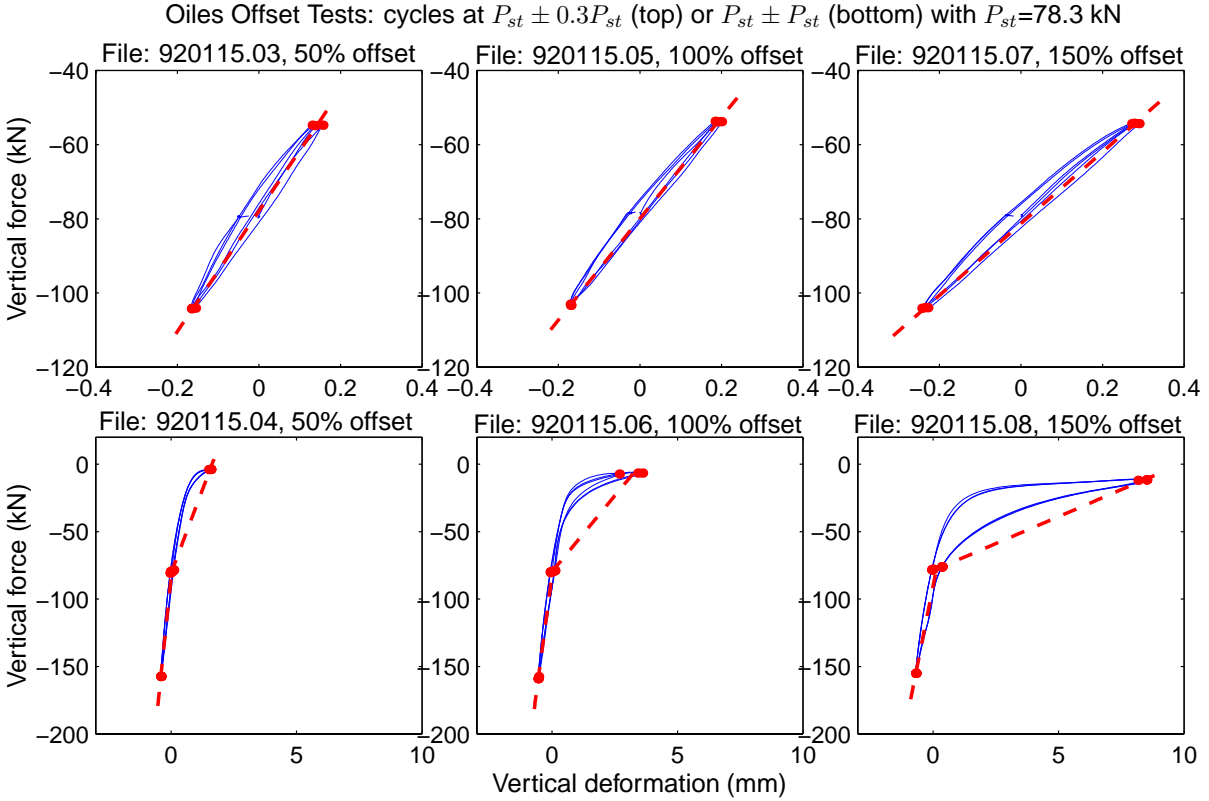


Figure 9: Vertical force-deformation for a single Oiles bearing at offset shear strains of 50, 100, 150% and load cycles of $P \pm 0.3P$ and $P \pm P$. Interpretation of vertical stiffness above and below the design load P given by dashed lines.

Vertical Stiffness

Shown separately for each bearing type, the resulting vertical stiffness determined from the offset tests is plotted as a function of lateral deformation \div bending radius (u_b/r_b) in Fig. 10. The observed stiffness k_{bz} has been normalized by the nominal stiffness k_{bz0} – the observed stiffness at zero shear strain – and is compared with the theoretical stiffness (Eq. 4), plotted as a solid line. The theoretical and experimental stiffness ratios are in good agreement for the Bridgestone bearings (Fig. 10a) and the Oiles LRB bearings (Fig. 10c). Unfortunately, the predicted reduction in stiffness does not agree with test data for the MR-PRA bearings (Fig. 10b), and currently we have no explanation for this discrepancy. (The difficulties in measuring vertical deformation should not significantly affect the *relative* stiffness ratio k_{bz}/k_{bz0}). However, evaluating the data set in toto, including both axial-load varied and offset tests, the experimental data provides a reasonable confirmation of the theory.

CONCLUSIONS

The following “axial load effects” have been observed from the bearing test data:

1. The lateral post-yield stiffness of both high-damping rubber bearings (Bridgestone and MRPRA) and lead-rubber bearings (Oiles) decreases with increasing axial load. For the Bridgestone and

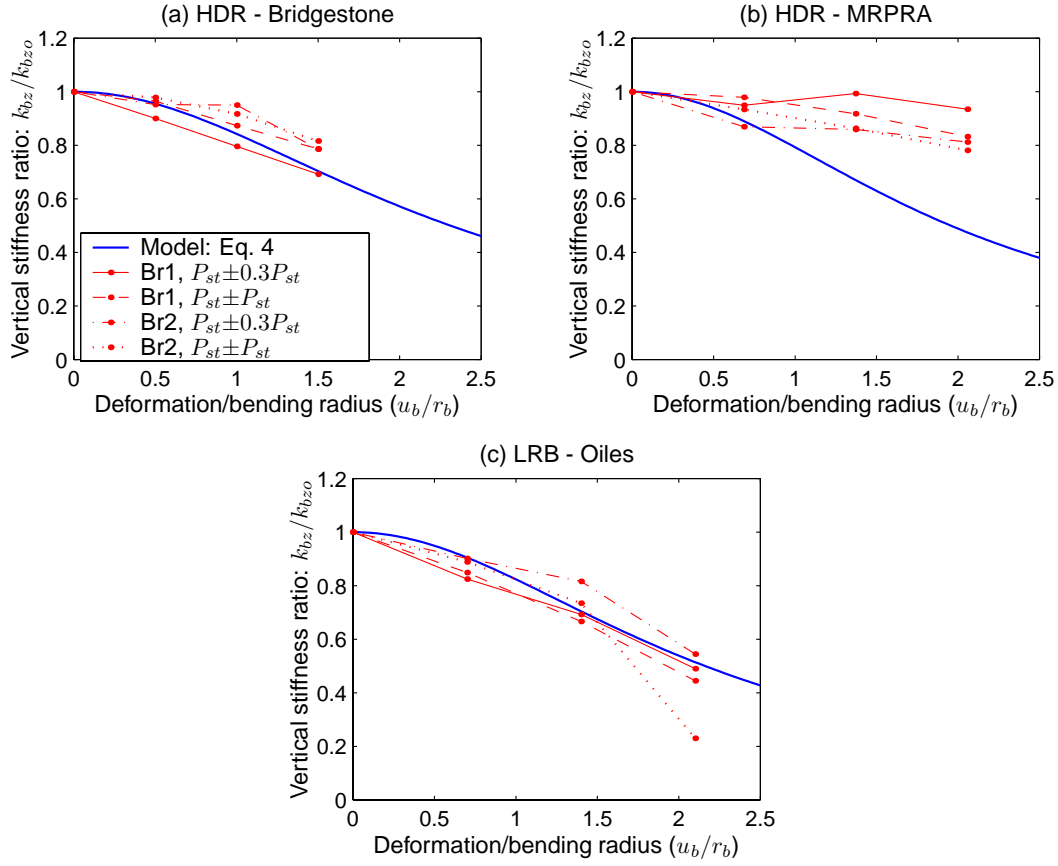


Figure 10: Vertical stiffness ratio k_{bz}/k_{bzo} vs u_b/r_b for (a) Bridgestone HDR, (b) MRPRA HDR, and (c) Oiles LRB. Experimentally observed values for two different bearings and two different load sequences are compared with Eq. 4. $P_{st}=78$ kN for Bearing 1 and 49 kN for Bearing 2.

MRPRA bearings, this decrease in stiffness is well-represented by Eq. 2, determined from linear stability analysis of a two-spring model of the bearing.

2. The lateral yield strength of the Oiles lead-rubber bearings decreases with decreasing axial load. This strength variation is well represented by Eq. 5, an empirical model developed to fit the experimental data.
3. The vertical stiffness of the three different bearings decreases as lateral deformation increases. The stiffness of the Bridgestone and Oiles bearings is well-represented by Eq. 4, determined from linear stability analysis of a two-spring model of the bearing.

These effects should be incorporated into a model for isolation bearings that can be used in dynamic analysis.

Vertical characteristic tests indicated that energy dissipation in the vertical direction can be modeled as viscous, with a damping coefficient between 5 and 10%. In our judgement, a damping coefficient of 5% in the vertical direction would be appropriate for dynamic analysis.

REFERENCES

1. Griffith MC, Kelly JM, Coveney VA, Koh CG. "Experimental evaluation of medium-rise structures subject to uplift." Earthquake Engineering Research Center, University of California, Berkeley, California. Rep. No.UCB/EERC-88/02, 1988.
2. Kelly JM, Buckle IG, Koh CG. "Mechanical characteristics of base isolation bearings for a bridge deck model test." Earthquake Engineering Research Center, University of California, Berkeley, California. Rep. No.UCB/EERC-86/11, 1986.
3. Aiken ID, Kelly JM, Tajirian FF. "Mechanics of low shape factor elastomeric seismic isolation bearings." Earthquake Engineering Research Center, University of California, Berkeley, California. Rep. No.UCB/EERC-89/13, 1989.
4. Clark PW, Aiken ID, Kelly JM. "Experimental studies of the ultimate behavior of seismically-isolated structures." Earthquake Engineering Research Center, University of California, Berkeley, California. Rep. No.UCB/EERC-97/18, 1997.
5. Kelly JM. "Tension buckling in multilayer elastomeric bearings." Journal of Engineering Mechanics (ASCE), 2003; 129(12):1363-1368.
6. Tyler RG, Robinson WH. "High-strain tests on lead-rubber bearings for earthquake loadings." Bulletin of the New Zealand National Society for Earthquake Engineering, 1984; 17(2):90-105.
7. Hwang J-S, Hsu T-Y. "Experimental study of isolated building under triaxial ground excitations." Journal of Structural Engineering (ASCE), 2000; 126(8):879-886.
8. Aiken ID, Kelly JM, Clark PW, Tamura K, Kikuchi M, Itoh T. "Experimental studies of the mechanical characteristics of three types of seismic isolation bearings." 10th World Conference on Earthquake Engineering. Rotterdam, AA Balkema, 1992; 4:2281-2286.
9. Kelly JM. Earthquake-Resistant Design with Rubber. Springer, 1997.